WELDING OF SINGLE CRYSTAL NICKEL-BASED SUPERALLOYS

J. M. Vitek, S. S. Babu, J-W. Park, and S. A. David
Oak Ridge National Laboratory
Oak Ridge, Tennessee, USA

Abstract

A series of laser welds were made at different weld speeds and powers on thin sheet samples of a single crystal nickel-based superalloy (Rene N5). The welds were evaluated by optical microscopy to identify the extent of stray grain formation. The welds were made along an asymmetric crystallographic direction and the micrographs showed that stray grain formation and associated cracking were also asymmetric with respect to the weld centerline. Furthermore, stray grain formation was more prevalent at higher weld speeds and weld power (but lower heat input). A thermal model was used to predict the weld pool shape for the different welding conditions and this model was used in conjunction with a geometric model to determine the dendrite solidification microstructure. The thermal model was also used to identify the variation in the thermal gradient along the weld pool solidification interface. The model results showed a clear correlation between the stray grain formation tendencies and the value of the parameter G^N/V (G=gradient, V=velocity, N=constant). The results agree very well with expectations based on the mechanism of constitutional supercooling for stray grain formation.

Introduction

High temperature demands on aircraft turbine engines have led to the extensive use of single crystal nickel-based superalloys over the last 20 years. The absence of grain boundaries in single crystal components results in improved creep properties which, in turn, allows for engine

operation at higher temperatures, thereby achieving improved engine efficiencies. The application of single crystal materials to larger land-based turbine engines is desired so that the same improvements in efficiency can be realized. Due to the intrinsic high cost of single-crystal engine components, especially for larger land-based turbine applications, there is a need to be able to weld these components in order to salvage imperfect as-cast components as well as to refurbish and repair worn or damaged parts. Welding of single crystal nickel-based superalloys is problematic due to the formation of new grains (known as stray grains) during weld solidification, leading to a loss of the single-crystal nature of the components and an associated loss in creep properties. A representative electron beam (EB) weld of a commercial PWA 1480 alloy is shown in Figure 1. The weld was made along the [100] direction on the (001) plane. There are regions where epitaxial growth is found, thus maintaining the single crystal structure. A few such regions are marked with black arrows that indicate the dendrite growth direction. However, numerous stray grains are visible and a few are highlighted with white arrows. Cracking is also evident and, as shown elsewhere,[1,2] the cracks often

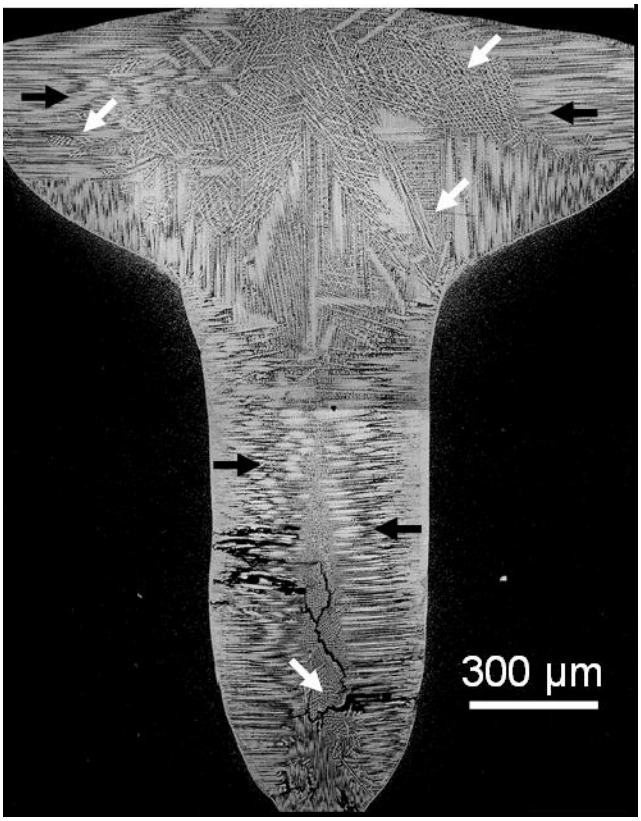

Figure 1: EB weld made along [100] direction and on (001) plane of commercial alloy PWA 1480 showing extensive stray grain formation (white arrows) and crack formation. A few regions with epitaxial dendritic growth, that retain the base metal single crystal orientation, are shown with black arrows pointing along dendrite growth direction.

follow the high angle grain boundaries associated with the stray grains. Such stray grain formation and cracking is commonplace in single-crystal nickel-based superalloys welded by a variety of processes, including GTA, laser, pulsed laser, and electron beam.[1,2] This paper will present a combination of recent experimental and modeling results that attempt to identify the mechanism of stray grain formation. Identification of the underlying mechanism should provide valuable insight as to how to avoid, or at least minimize, stray grain formation and associated cracking during weld repair operations.

Experimental Procedure

Autogenous laser welds were produced on thin sheets (25.4 mm x 50 mm x 0.8 mm) of a Rene N5 alloy. The composition of this alloy is Ni-6.25Al-7.32Co-7.11Cr-6.38Ta-4.83W-2.88Re-1.41Mo-0.15Hf-0.053C (wt %). A 1.5 kW continuous wave Nd-YAG laser was used with argon gas shielding. Three different combinations of processing conditions were used (see Table I). In going from Weld A to C, the weld speed and power were increased while the heat input (power ÷ speed) was decreased. The welding direction was along the longitudinal direction of the original cast plate from which the thin sheet was cut and the welding plane was parallel to the original cast plate surface. The weld direction and sheet normal were measured using Laue

Table 1: List of welding conditions used for single crystal Rene N5 thin sheet samples.

	Weld A	Weld B	Weld C
Power (W)	420	804	840
Velocity (mm/s)	4.2	12.7	21.2
Heat Input (J/mm)	100	63.3	39.6

diffraction and were determined to be [0.141, $\overline{0.217}$, 0.966] and [$\overline{0.925}$, $\overline{0.376}$, 0.051], respectively. These directions correspond to deviations of 15° and 22° from the [0 0 1] and [$\bar{1}$ 0 0] directions, respectively.

Transverse and top surface mounts were prepared from the three welds and they were polished and etched for optical microscopy. In combination with the geometric dendrite growth model, described later, the dendritic orientations were identified from micrographs of these sections. Also, the degree of stray grain formation in the top sections of the welds was identified by orientation imaging microscopy (OIM).

Three-dimensional thermal modeling of the laser welding process was done by using Sysweld®,[3] a commercial finite element code for welding problems. Temperature dependent material properties were used,[4] and heat loss on the surface by convection and radiation was considered. The shape of the heat source was adjusted so that the predicted and experimental weld cross-sections were in agreement.[4] In addition, the shape of the heat source was modified so that the transition points between zones of different dendritic growth orientations, calculated from the simulated weld pool shape and the geometric growth model described later, agreed with the experimental results. The latter heat source adjustments were only minor, and affected the heat source shape only in the welding direction, so that they could be made without compromising the weld cross-section fitting.

A geometric model[5,6] was used to describe the selected dendrite growth direction as a function of the solidification front direction and the sample's crystallographic orientation. The model is based on the premise that epitaxial dendritic growth is along one of the six <100> preferred growth directions,[7-9] and that the active dendritic growth direction at any given location along the solidification front is the variant with the minimum undercooling, or equivalently, the minimum growth velocity. This geometric model has been verified by extensive examination of welds made on a model Fe-15Cr-15Ni alloy where stray grain formation was absent and confirmation of the model was possible.[5,6,10,11] Figure 2 is a schematic diagram that describes the basic parameters and approach used in this geometric model. A fixed set of reference axes is defined (x, y, z) where the weld direction is in the positive x direction. At any given location along the weld solidification front, one can define the solidification front normal direction, $\vec{\mathbf{n}}$ in terms of the two angles θ and φ (see Figure 2). Another angle, ψ, is defined as the angle between $\vec{\mathbf{n}}$ and $\vec{\mathbf{V}}_{hkl}$, which is parallel to the dendrite growth direction. The dendrite growth velocity $\vec{\mathbf{V}}_{hkl}$ can be expressed in terms of θ, φ, and the weld

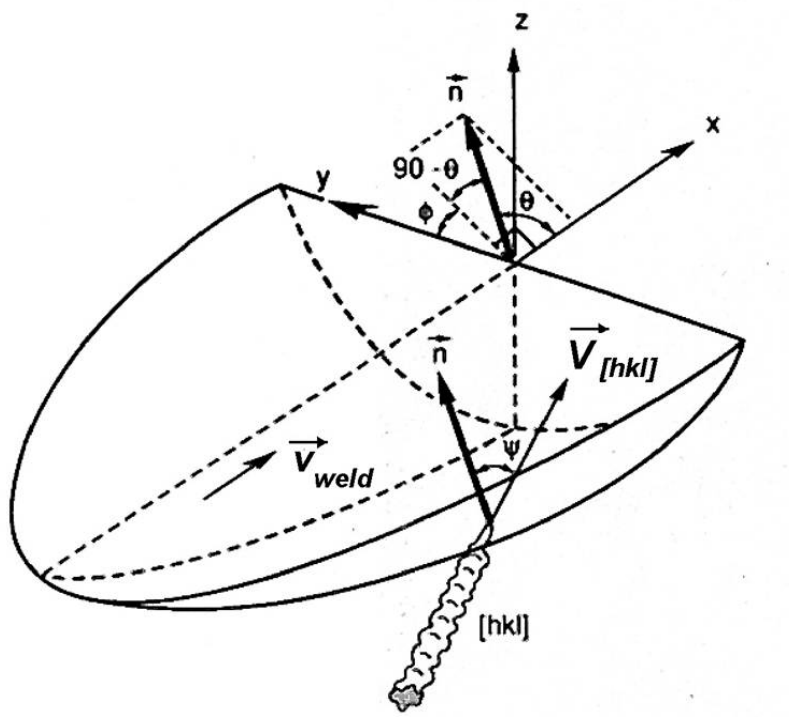

Figure 2: Schematic diagram showing the basic elements of the analysis using the geometric model (see text for description of various quantities).

velocity $\vec{\mathbf{V}}_{weld}$, as[5]:

$$\left|\vec{V}_{hkl}\right| = \left|\vec{V}_{weld}\right| \frac{\cos\theta}{\cos\varphi} \qquad \textbf{(1)}$$

It can also be shown[5] that the dendrite growth velocity is related to the solidification front growth velocity in the direction $\vec{\mathbf{n}}$, $\vec{\mathbf{V}}_n$, by:

$$\left|\vec{V}_{hkl}\right| = \frac{\left|\vec{V}_n\right|}{\cos\psi} \qquad \textbf{(2)}$$

The active dendrite growth direction at any given location is the direction with the minimum undercooling, which corresponds to the minimum growth velocity, and represents the <100> variant that is most closely aligned with the solidification front normal. Since the solidification front normal orientation varies continuously across the weld pool surface, a set of zones will be defined as a function of θ and φ that correspond to regions of different active dendrite growth directions. It should be kept in mind that in spite of the presence of such zones of different dendrite orientations, the overall single crystal nature of the base material is maintained as long as only the six <100> variants of the base material are active and no new (stray) grains form.

The geometric and thermal models were used to determine the thermal gradients along the solidification front. The maximum thermal gradient at any given location, $\vec{\mathbf{G}}_n$, is parallel to the solidification front normal and its magnitude can be expressed in terms of the components of $\vec{\mathbf{G}}_n$ along the three reference axes, G_x, G_y, and G_z , as $\sqrt{G_x^2 + G_y^2 + G_z^2}$. The values of G_x, G_y, and G_z were determined from the thermal model and used to calculate θ and φ with the help of the following relationships:

$$\theta = \cos^{-1}\left(\frac{G_x}{\left|\vec{G}_n\right|}\right) \qquad \varphi = \cos^{-1}\left(\frac{G_y}{\left|\vec{G}_n\right|\sin\theta}\right) \tag{3}$$

The thermal gradient along the dendrite growth direction, $\vec{\mathbf{G}}_{\text{hkl}}$, is given by the expression:

$$\left|\vec{G}_{hkl}\right| = \left|\vec{G}_n\right|\cos\psi \tag{4}$$

The angle ψ can be calculated at all locations if $\vec{\mathbf{n}}$ and the active dendrite growth direction [hkl] are known. Since the active dendrite growth direction is the variant most closely aligned with the solidification front normal, it is also the variant with the minimum value of ψ and the maximum thermal gradient. The temperature gradient along the active dendrite growth direction $\vec{\mathbf{G}}_{\text{hkl}}$ was calculated along the entire solidification front for the x-z plane 0.05 mm below the top free surface, which approximately corresponds to the metallographic top surface section position after taking into account the material that was removed during polishing.

Results

Transverse and surface view optical micrographs of the laser welds are shown in Figures 3-5 for the three welding conditions. Several features are noteworthy. First, as shown in the surface views, there are no transverse cracks in the 4.2 mm/sec laser weld while transverse cracks were present in the 12.7 and 21.2 mm/sec welds. Second, the cracking behavior was clearly asymmetrical with respect to the weld centerline in that nearly all the cracks were located on one side of the centerline. Third, there are distinct zones of dendrite growth orientations that represent different <100> dendrite growth variants. For example, a change in dendrite growth direction can be seen clearly in Figure 3b, where nearly transverse-oriented dendrites are replaced by nearly longitudinal-oriented dendrites about 300μm from the right edge of the weld

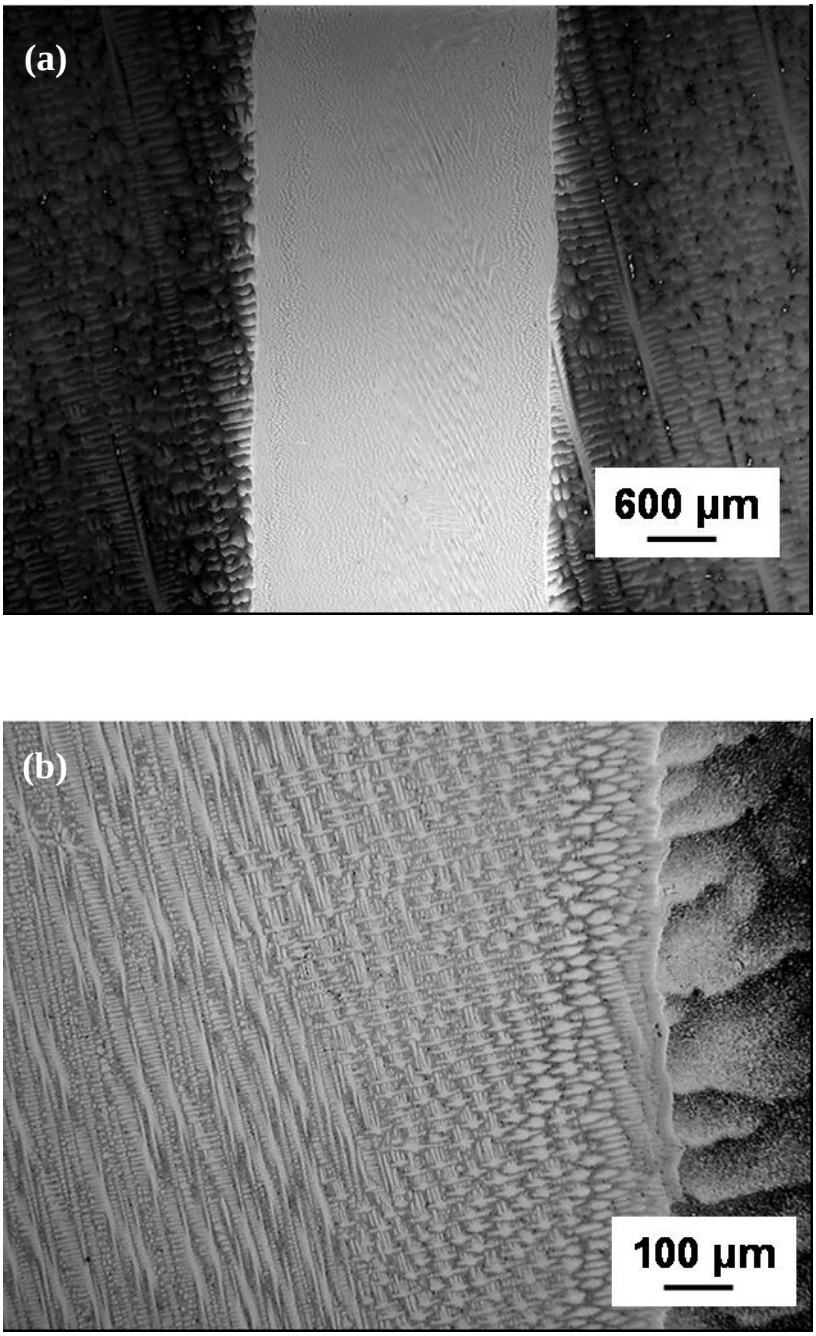

Figure 3: Optical micrographs of laser weld “A” (4.2 mm/s): (a) low magnification top surface view, (b) higher magnification top surface view, (c) low magnification transverse view and (d) higher magnification transverse view.

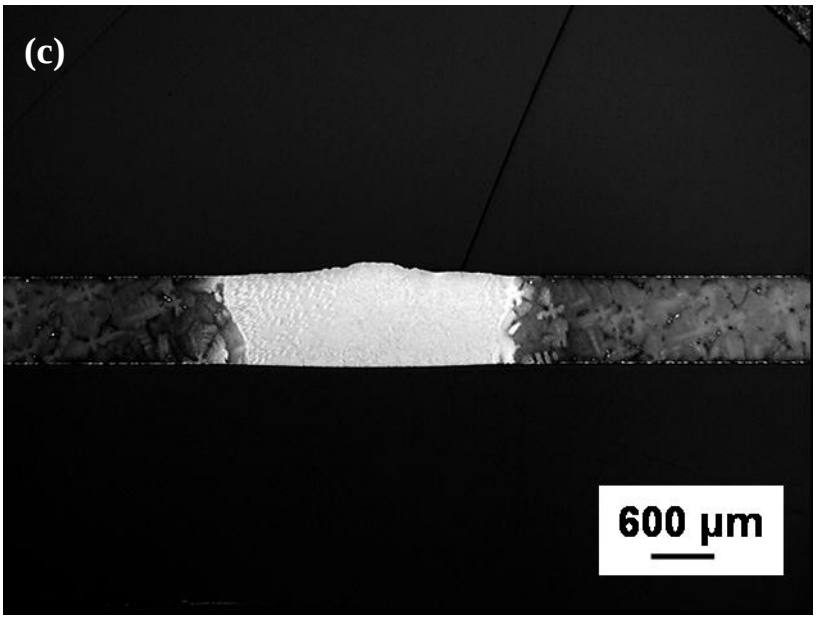

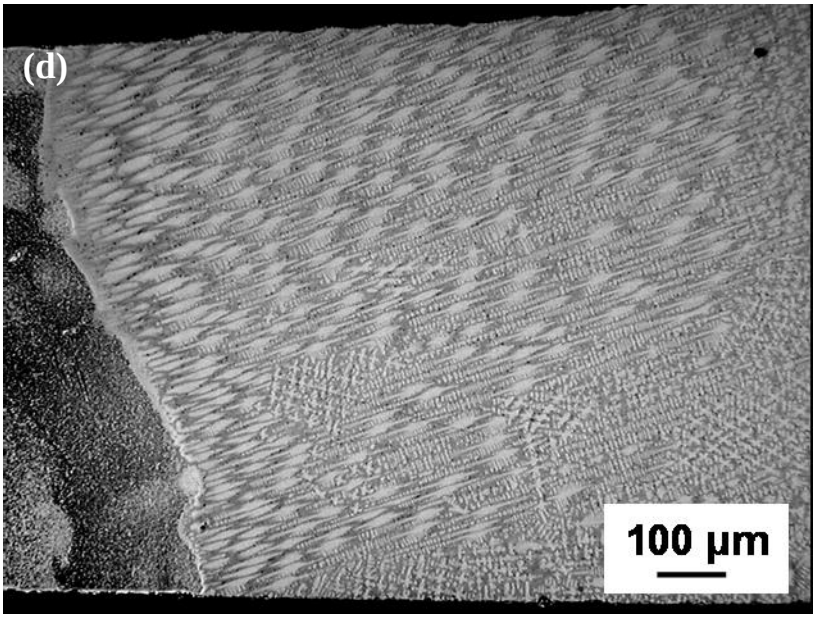

Figure 3 (cont): Optical micrographs of laser weld "A" (4.2 mm/s): (a) low magnification top surface view, (b) higher magnification top surface view, (c) low magnification transverse view and (d) higher magnification transverse view.

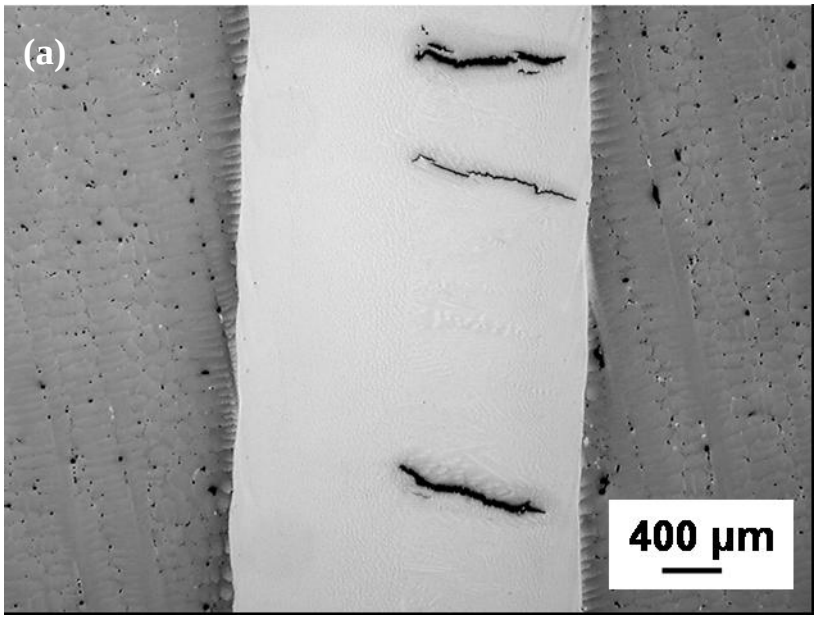

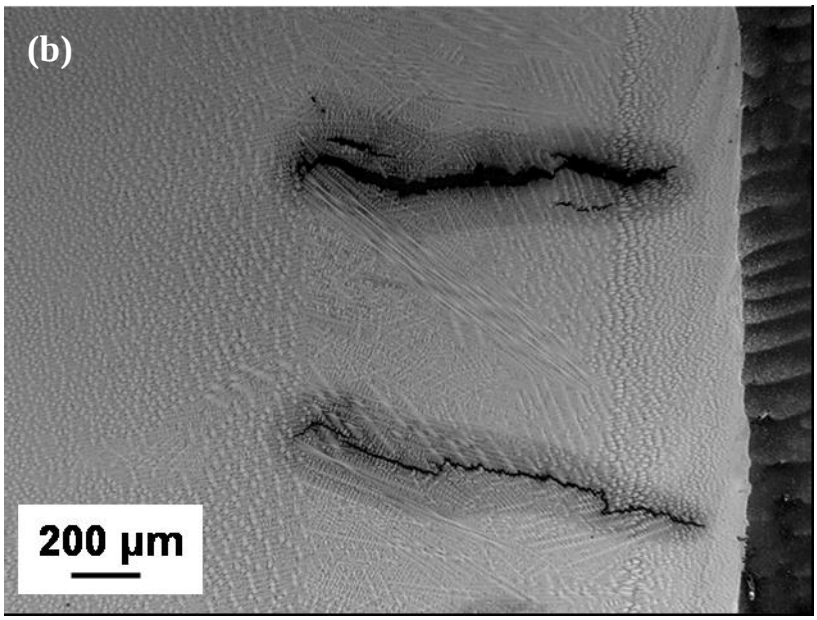

Figure 4: Optical micrographs of laser weld "B" (12.7 mm/s): (a) low magnification top surface view, (b) higher magnification top surface view, (c) low magnification transverse view and (d) higher magnification transverse view.

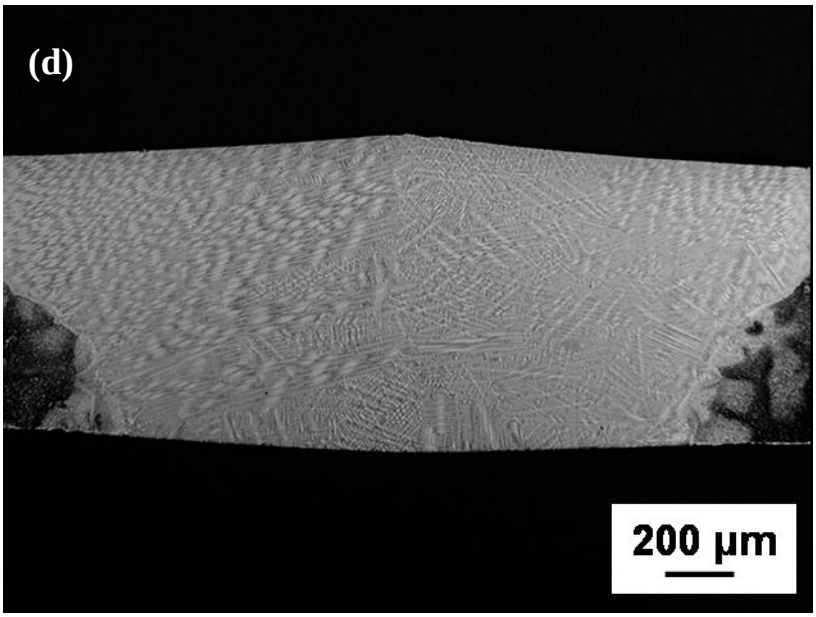

Figure 4(cont): Optical micrographs of laser weld “B” (12.7 mm/s): (a) low magnification top surface view, (b) higher magnification top surface view, (c) low magnification transverse view and (d) higher magnification transverse view.

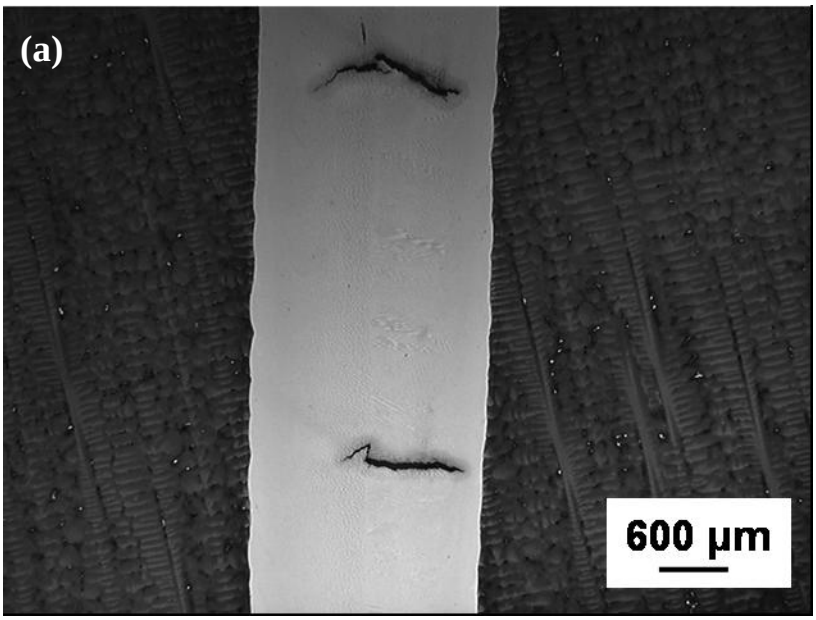

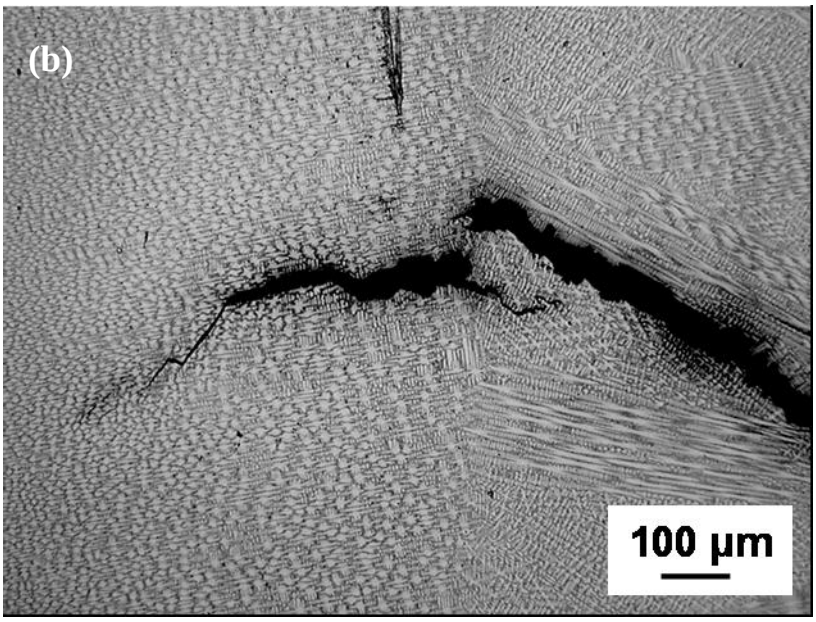

Figure 5: Optical micrographs of laser weld "C" (21.2 mm/s): (a) low magnification top surface view, (b) higher magnification top surface view, (c) low magnification transverse view and (d) higher magnification transverse view.

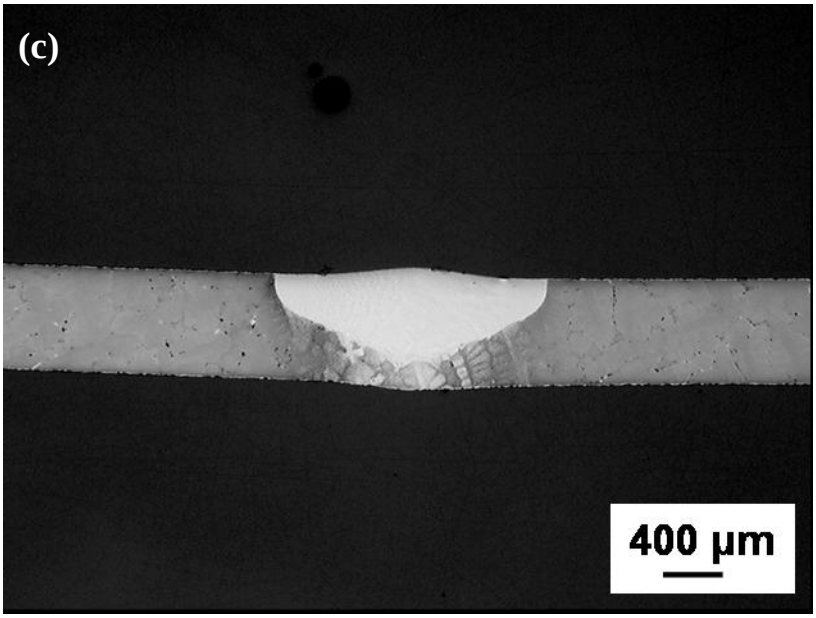

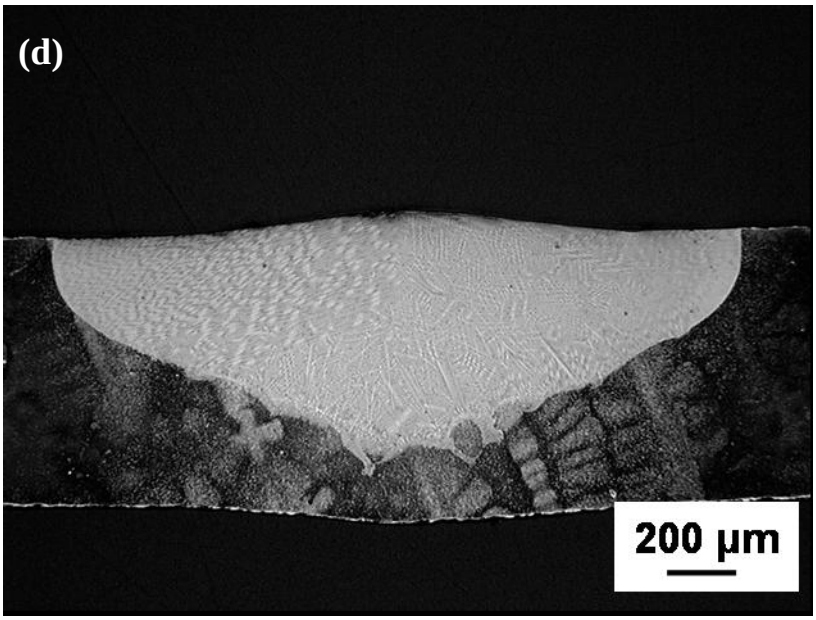

Figure 5(cont): Optical micrographs of laser weld “C” (21.2 mm/s): (a) low magnification top surface view, (b) higher magnification top surface view, (c) low magnification transverse view and (d) higher magnification transverse view.

pool. Fourth, the higher magnification views show the presence of stray grains in all welds (Figures 3d, 4b, 4d, 5b and 5d), but the number of stray grains increases noticeably with welding speed. Fifth, the higher magnification views also show that the stray grains are not symmetrically distributed about the weld centerline; there are clearly more stray grains on the right side, the same side that the cracking is found. This is most clearly shown in Figures 4d and 5d. Finally, the cracks tend to lie along the stray grain (high angle) boundaries (Figures 4b, 5b).

Results from OIM analysis of the three welds are shown in Figure 6. The OIM procedure creates a 2D map of the crystallographic orientation of the welds and from this information the location of high angle grain boundaries were determined. The OIM analysis confirms the observations made on the optical micrographs, namely, more stray grains (more high-angle boundaries) are found as the weld speed increases, the stray grains are much more abundant on one side of the weld, and the cracks follow along the stray grain boundaries. It is also noteworthy that the distinct dendrite zones that represent different <100> growth direction variants related to the base material orientation are not separated by high angle boundaries because they all represent the same single crystal orientation.

The asymmetry with respect to the weld centerline in the dendrite growth patterns can be readily explained by using the geometric model for the specific weld direction and surface normal used in this study. A map of the dendrite growth zones as a function of θ and φ is shown in Figure 7. Referring to the schematic diagram in Figure 2, $\varphi = 90°$ represents the weld centerline and the right side of the weld corresponds to $0° < \varphi < 90°$ while the left side corresponds to $180° > \varphi > 90°$. Superimposed on the figure is a heavy dotted line that represents the calculated values for θ

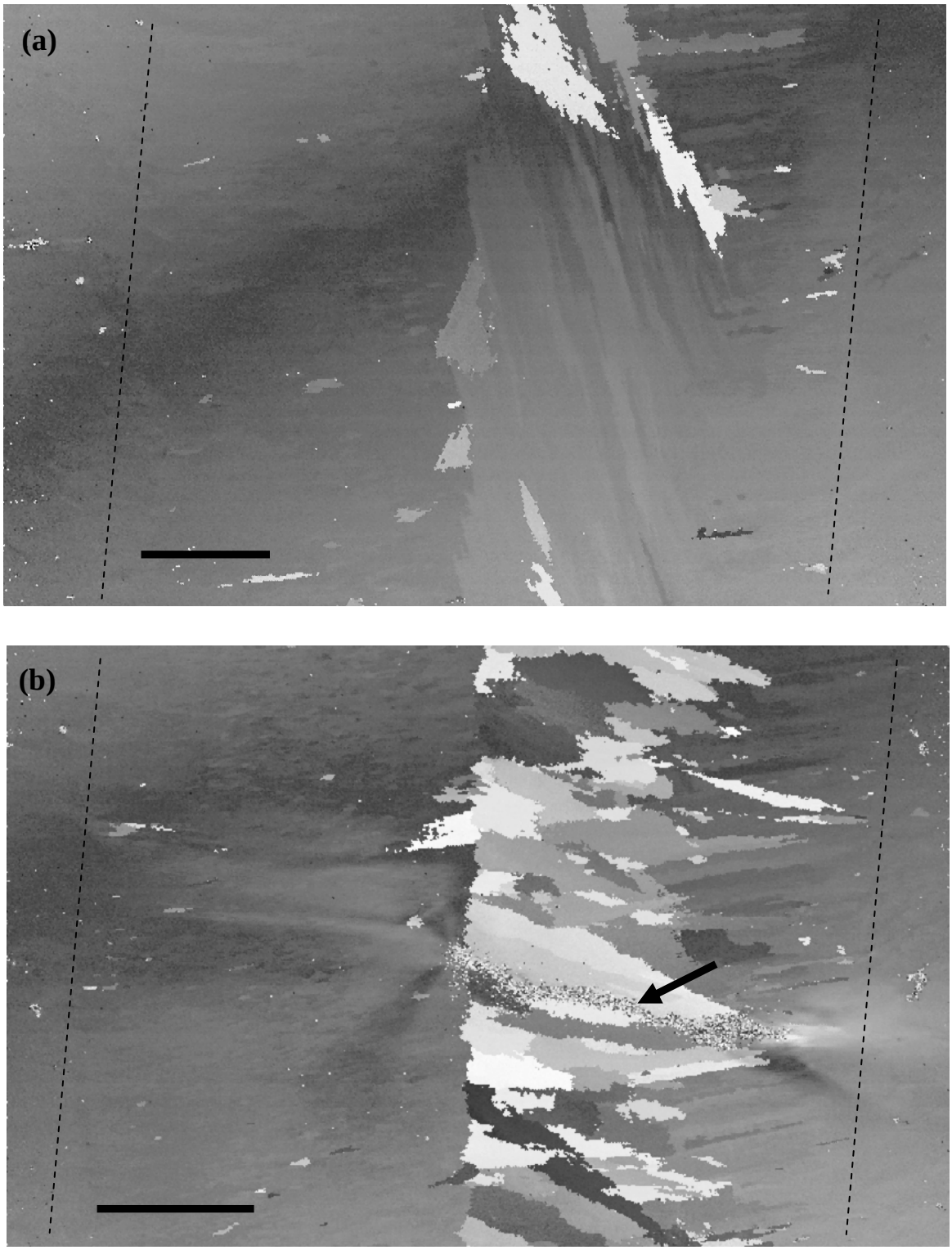

Figure 6: Surface-view micrographs showing different grains in welds as determined by OIM analysis. The dashed lines represent approximate weld boundaries and the scale markers represent 500 µm. (a) Weld A, (b) Weld B, and (c) Weld C. Arrows indicate the location of cracks.

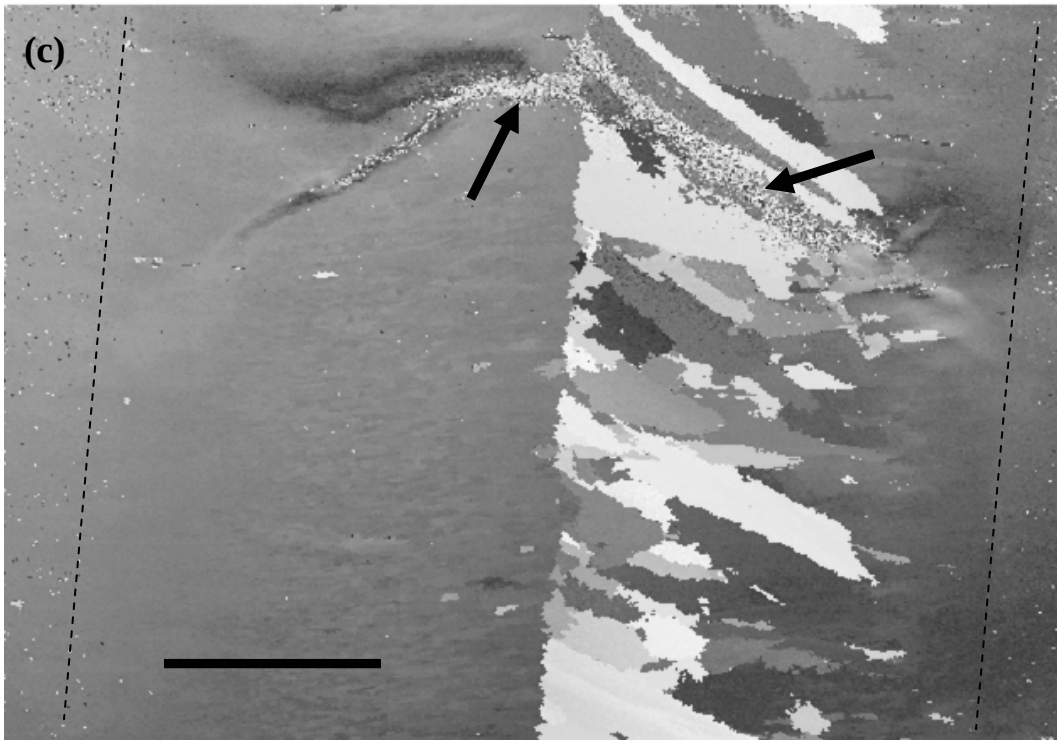

Figure 6(cont): Surface-view micrographs showing different grains in welds as determined by OIM analysis. The dashed lines represent approximate weld boundaries and the scale markers represent 500 µm. (a) Weld A, (b) Weld B, and (c) Weld C. Arrows indicate the location of cracks.

and φ along the fusion line for the low speed weld at a distance of 0.05 mm from the top, which corresponds to the approximate depth of the surface views and to the depth that was investigated further in the next section. Details as to the method used to calculate the orientation of the fusion line at this depth are presented elsewhere.[12] It is clear that the dendrite growth zones are asymmetrically distributed about the weld centerline. As discussed later, this asymmetry is directly responsible for the asymmetric stray grain formation and cracking tendencies. For example, along the fusion line, $[0\bar{1}0]$ dendrites are expected to exist over a major portion of the left side of the weld ($\varphi > 90°$) while dendrites growing in the opposite direction, [010], will only exist over a small portion of the right side of the weld ($\varphi < 90°$). Instead, [001] dendrites will be

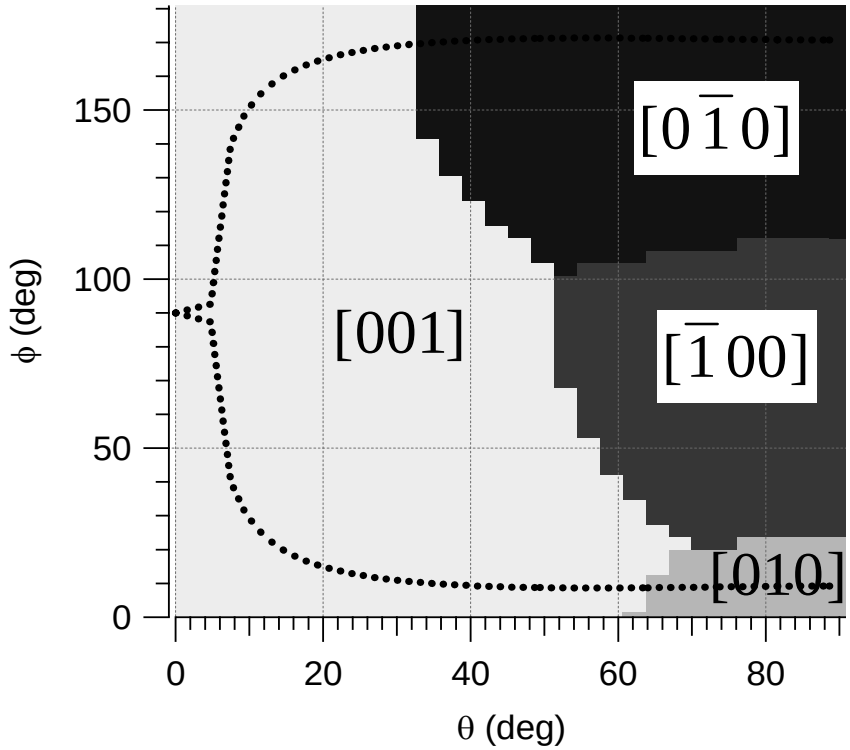

Figure 7: Calculated results from the geometric model showing the change in active dendrite growth direction as a function of the parameters θ and φ that define the weld pool surface orientation (see Figure 2). The calculations are for the specific crystallographic weld direction and weld surface orientation used in this study. The dotted line represents the weld pool interface orientation for Weld "A" at a depth of 0.05 mm, corresponding to the position of the top-surface micrographs in Figures 3a, 3b, and 6a.

present over a larger portion of the weld on the right side. The interplay between the active dendrite growth directions and their alignment with the solidification front normal along the weld pool interface determines the dendrite growth velocities and the gradients.

Discussion

The experimental work indicates that stray grain formation, and associated cracking, are common in the N5 alloy welds, similar to results for welds on other single crystal nickel-based superalloys.[1,2] However, in those sections of the welds where stray grains were absent and epitaxial growth from the base metal was found, the dendrite growth directions were in good agreement with those predicted by the geometric model. Thus, in agreement with earlier conclusions,[1,2,5,6,10,11] the geometric model is an accurate means for identifying the growth behavior during solidification of single crystals. Application of the geometric model also indicates that the size and shape of the zones of different active dendrite growth directions are

very sensitive to the exact weld pool shape. Thus, to the extent that the zones can be identified in spite of the presence of stray grains, the dendritic growth pattern can be used in conjunction with thermal modeling to accurately predict the 3D weld pool shape.

The primary objective of this paper is to evaluate the results in order to identify the mechanism of stray grain formation. One theory for stray grain formation, as applied to the evaluation of the columnar to equiaxed transition, is based on the principle of constitutional supercooling ahead of the advancing dendritic growth front.[13,14] According to this mechanism, the liquid immediately ahead of the advancing dendritic growth front will be undercooled since the dendrite tips themselves are undercooled. Depending upon the extent of this undercooling, and the thermal gradient and solute field in front of the dendrites, the conditions may be favorable for nucleation and growth of equiaxed grains ahead of the advancing dendritic solidification front. The extent of nucleation and growth of new, equiaxed grains will determine if the solidification morphology remains directionally oriented dendritic (no stray grains), or if it is a mixed dendritic/equiaxed microstructure, or if it converts completely to an equiaxed structure. The theories of Hunt[13] and Gaümann et al[14] show that the directional dendritic morphology can be maintained if the following relationship is satisfied:

$$\frac{G^N}{V} > K \qquad \textbf{(5)}$$

Here N and K are material-dependant constants and vary according to the analysis used to determine the dendrite tip undercooling. The values of these two constants have not been evaluated for the Rene N5 alloy used in this investigation since many of the parameters that are used to evaluate the constants are not known very well. However, values of N of 2 and 3.4 have

been proposed by Hunt[13] and Gaümann et al,[14] respectively, and the value of 3.4 used by Gaümann et al was for a commercial CMSX4 nickel-based superalloy which is quite similar to the alloy studied here. Equation (5) is not that different from the simple constitutional supercooling condition used to describe nucleation ahead of an advancing planar front, i.e., $G/V > \Delta T/D$ where ΔT is the solidification temperature range and D is the diffusion coefficient in the liquid. This latter relation was used qualitatively to describe stray grain formation tendencies.[2,15]

The thermal model was used to evaluate G^N/V in the x-y plane at a depth of 0.05 mm, which was estimated to be the position of the surface micrographs in Figures 3-5. The values of G and V were resolved along the dendrite growth directions and not along the solidification front normal, i.e., $\left|\vec{G}_{hkl}\right|$ and $\left|\vec{V}_{hkl}\right|$ were used rather than $\left|\vec{G}_n\right|$ and $\left|\vec{V}_n\right|$ (see Equations (2) and (4)). Therefore, they were dependent upon the actual dendrite growth direction. In order to evaluate G and V, the active dendrite growth directions and the solidification front normal orientations were determined from the geometric and thermal models, using Equations (1)-(4). Plots of G^N/V for various values of N are shown in Figure 8. Since the Rene N5 alloy is similar to the CMSX4 alloy used in the study by Gaümann et al,[14] the value of $N = 3.4$ may be most appropriate for the present case. In any event, it can be seen that the values of G^N/V are not symmetrical about the centerline. This is a direct consequence of the fact that the dendrite growth directions were not symmetrical about the weld centerline. It can be seen that except in the immediate vicinity of the weld centerline, regardless of the value of N, the values of G^N/V are smaller on the right side (dashed line), where stray grains are observed, than on the left side

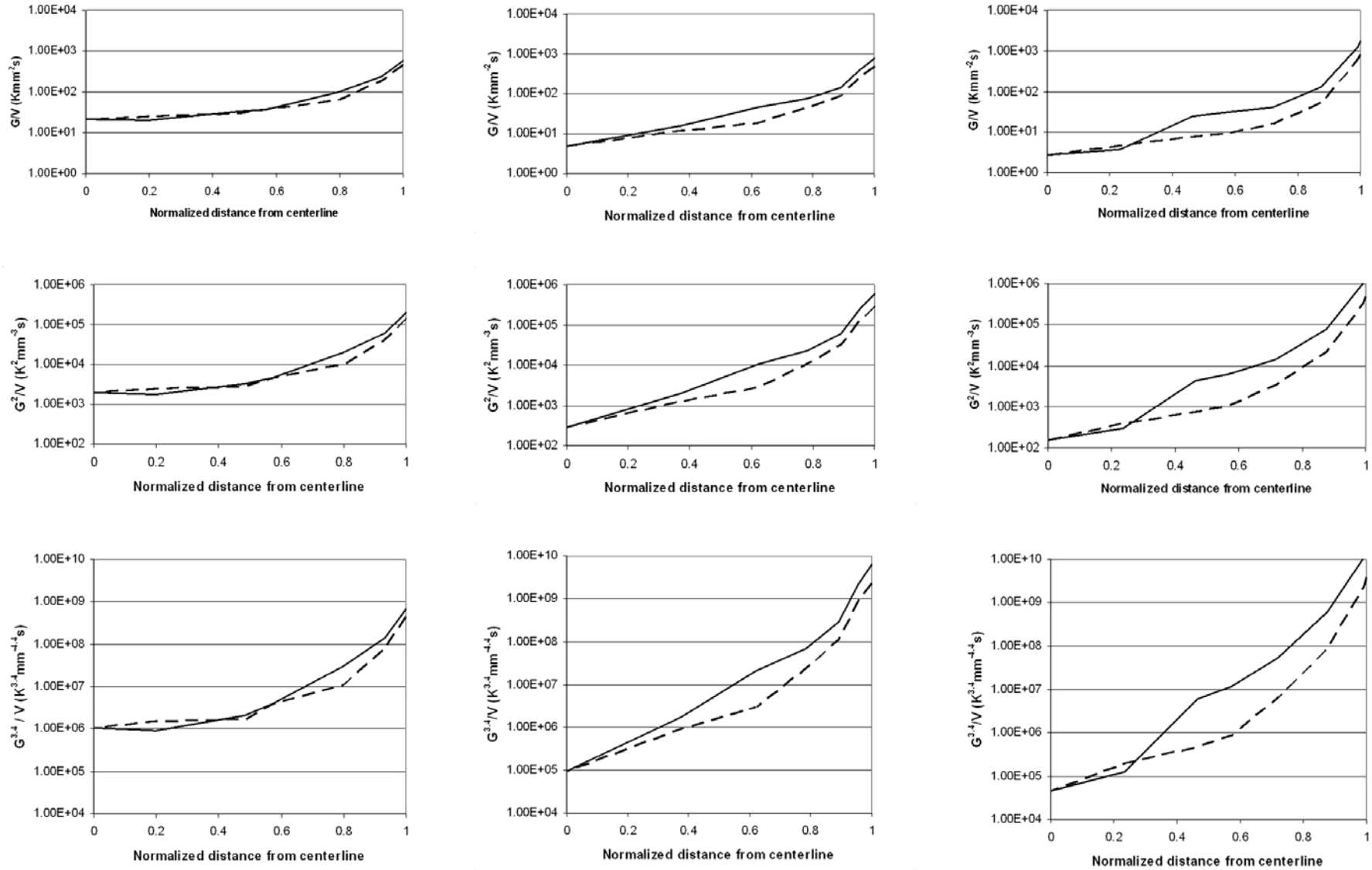

Figure 8: Plots of G^N/V versus normalized distance from the weld centerline for welds A, B, and C (columns 1, 2, 3, respectively) and for three different values of the constant N in Equation (5) (N=1, 2, 3.4 in rows 1, 2, 3, respectively). Values of G and V represent $\left|\vec{G}_{hkl}\right|$ and $\left|\vec{V}_{hkl}\right|$ so that variations in thermal properties as well as dendrite growth directions are taken into account. The solid lines are for the left side of the welds and the dashed lines are for the right side, where stray grain formation and cracking were more abundant.

(solid line). Furthermore, in all cases, the values of G^N/V decrease as the weld centerline is approached, and the values near the centerline are lower for any given N as the weld speed increases (reading left to right in Figure 8). According to Equation (5), low values of G^N/V promote the nucleation of new grains (stray grains), and the low values of G^N/V are found exactly where stray grains were observed experimentally, i.e., on the right side, near the centerline, and in higher speed welds. The differences in G^N/V between the left and right side become more pronounced as N increases (reading from top to bottom in Figure 8). Considering the case of $N = 3.4$ (bottom row in Figure 8), and using a somewhat arbitrary value of $K = 10^6$ in Equation (5), G^N/V is above K for nearly the entire weld at the lowest speed, and drops below K for the other two welds. Furthermore, it is below K for a significantly larger portion of the weld for the right side of the weld, especially for the highest speed weld. Thus, the theoretical criterion for avoiding stray grain formation (Equation (5)) fits the experimental observations very well.

An alternative mechanism for stray grain formation has been advanced by Pollock et al.[16] This mechanism is based on the hypothesis that stray grains form as a result of fluid flow motion and fragmentation of existing dendrites. The theory predicts that stray grain formation will tend to be related to the cooling rate, which is equivalent to the product GV. As the cooling rate decreases, the stray grain formation tendencies will increase. The thermal model was used to determine the values of GV for the three different weld conditions and the results are plotted in Figure 9. The results show that the experimentally observed stray grain formation tendencies do not correlate at all with the cooling rate values. First, the solution of the heat flow problem is independent of

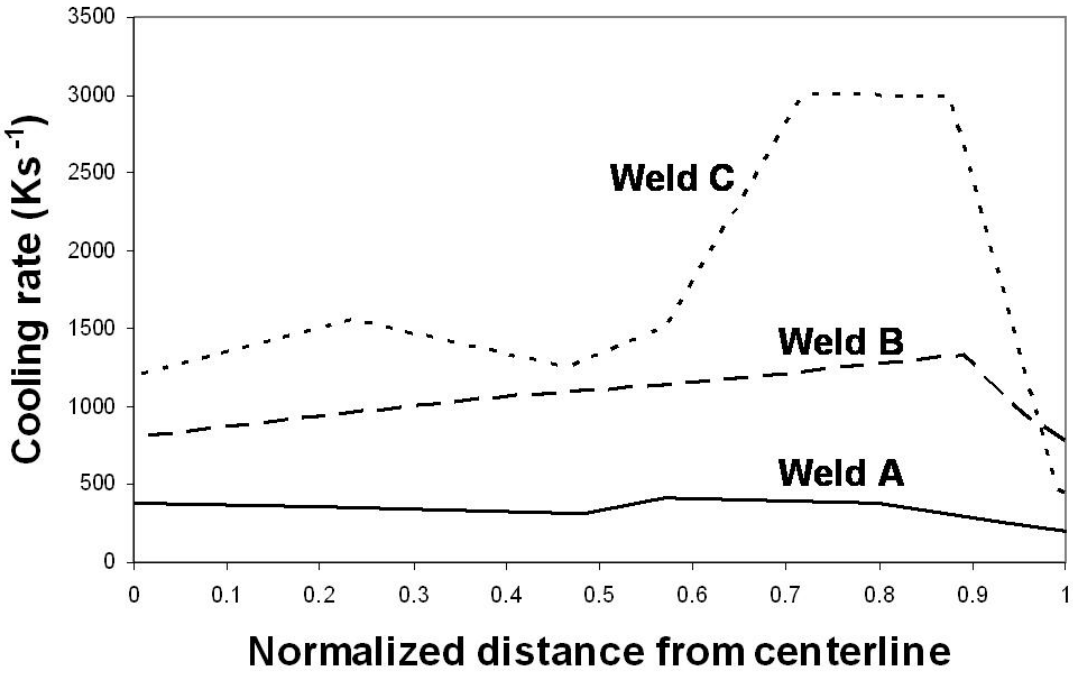

Figure 9: Plots of cooling rate (GV) versus normalized distance from the weld centerline for welds A, B, and C. G and V were calculated using the thermal model. Cooling rate is symmetrical about the weld centerline so it is the same for both the left and right sides.

dendrite growth orientation so that the values of GV are symmetrical about the weld centerline, in direct contrast to the well-pronounced asymmetry of stray grain formation that was found experimentally. Second, the cooling rate is fairly uniform across the weld, with a slight tendency for it to decrease near the outer edge. Thus, the stray grains should be most abundant near the outer edge but this is contrary to what was not found experimentally. Finally, cooling rates are least for Weld "A", implying this would be the weld that should be most prone to stray grain formation, but this was not observed. Thus, the predictions of the fragmentation model do not agree with the experimental findings for laser welds. It must be noted that the gradients, growth rates, and cooling rates during welding are quite different than those during conventional casting,

and it is possible that one mechanism (constitutional supercooling) prevails during welding while the other mechanism (fragmentation) prevails during casting.

Finally, it is worthwhile making some general comments on the potential for successfully welding single crystals and maintaining the single crystal structure. The experimental observations show that stray grain formation and associated cracking, although commonplace in nickel-based superalloys, can be avoided if the conditions are correct. The present results indicate that the constitutional supercooling mechanism, and in particular the criterion G^N/V, appears to be a valid parameter for identifying stray grain formation tendencies. However, optimization of welding parameters may be quite complex. Even with the G^N/V criterion, one must consider the actual G and V along the dendrite growth direction and so the weld orientation, and the change in weld pool shape with changing weld velocity and weld power, must all be taken into account. As shown in the experimental welds, the orientation of the single crystal can have a dramatic effect in terms of avoiding or reducing stray grains and cracks. Combining Equations (1) and (2) into Equation (5), one can see that

$$\frac{G^N}{V} = \frac{\left|\vec{G}_n\right|^N}{\left|\vec{V}_n\right|} \cos^{N+1}\psi \qquad \textbf{(6)}$$

Thus, successful welds will require high values of G^N/V. This condition means high values of ψ and $\vec{\mathbf{V}}_n$ and low values of $\vec{\mathbf{G}}_n$ must be avoided across the entire weld pool solidification interface. The weld configuration also plays an important role. For example, successful welds have been made on single crystals in a cladding-type configuration, in which the thermal gradients are uni-directional.[17] This is in contrast to welds in a groove or crack, in which the

thermal flow direction is from the sides as well as from the bottom, similar to the conditions in this study. In these configurations, the thermal gradients vary to a greater degree across the entire weld front. Optimization of welding conditions and parameters will require detailed thermal analysis of the weld pool as a function of weld orientation.

Summary

Laser welds were made on single crystal Rene N5 thin sheet samples. The welds were made along an asymmetric crystallographic direction and the resultant microstructures were also asymmetric with respect to stray grain formation and associated cracking. The results showed that stray grain formation is sensitive to the welding conditions as well as the crystal orientation. Extensive thermal modeling, coupled with a geometric model to describe the variation of active dendritic growth directions across the weld, was used to identify the conditions that promote stray grain formation. It was found that stray grain formation tendencies increased as the parameter G^N/V decreased (G=thermal gradient and V=dendrite growth velocity, both resolved along the dendrite growth direction, and N=constant). These results are in good agreement with a proposed mechanism for stray grain formation based on constitutional supercooling ahead of the growing dendrite front. The results do not agree with expectations based on a dendrite fragmentation mechanism for stray grain formation in laser welds.

Acknowledgments

This research was sponsored by the Office of Fossil Energy, DOE National Energy Technology Laboratory, and the Division of Materials Sciences and Engineering, U. S. Department of

Energy, under contract DE-AC05-00OR22725 with UT-Battelle, LLC. The authors would like to thank General Electric Corporation for supplying the Rene N5 material and R. W. Reed, Jr. for preparing the welds.

References

1. S. A. DAVID, J. M. VITEK, S. S. BABU, L. A. BOATNER and R. W. REED: 'Welding of Nickel Base Superalloy Single Crystals', *Sci. Technol. Welding Joining*, 1997, **2** (2), 79-88.
2. J. M. VITEK, S. A. DAVID AND L. A. BOATNER: 'Microstructural Development in Single Crystal Nickel Base Superalloy Welds', *Sci. Technol. Welding Joining*, 1997, **2** (3), 109-118.
3. Sysweld, ver. 2002, ESI, Detroit, MI.
4. D. DYE, O. HUNZIKER, S. M. ROBERTS and R. C. REED: 'Modeling of the Mechanical Effects Induced by the Tungsten Inert-Gas Welding of the IN718 Superalloy', *Metall Mater. Trans A*, 2001, **32A**, 1713-1725.
5. M. RAPPAZ, S. A. DAVID, J. M. VITEK and L. A. BOATNER: 'Development of Microstructures in Fe-15Ni-15Cr Single Crystal Electron Beam Welds', *Metall Trans A*, 1989, **20A**, 1125-1138.
6. M. RAPPAZ, S. A. DAVID, J. M. VITEK and L. A. BOATNER: 'Analysis of Solidfication Microstructures in Fe-Ni-Cr Single-Crystal Welds', *Metall Trans A*, 1990, **21A**, 1767-1782.
7. M. C. FLEMINGS: *Solidification Processing*, McGraw-Hill, New York, 1974, p. 159.

8. W. KURZ and D. J. FISHER: *Fundamentals of Solidification*, Trans Tech Publications, Aedermannsdorf, Switzerland, 1984, p. 240.

9. M. RAPPAZ and E. BLANK: 'Simulation of Oriented Dendritic Microstructures Using the Concept of Dendritic Lattice', *J Cryst Growth*, 1986, **74,** 67-76.

10. S. A. DAVID, J. M. VITEK, M. RAPPAZ and L. A. BOATNER: 'Microstructure of Stainless Steel Single-Crystal Electron Beam Welds', *Metall Trans A*, 1990, **21A**, 1753-1766.

11. M. RAPPAZ, J. M. VITEK, S. A. DAVID and L. A. BOATNER: 'Microstructural Formation in Longitudinal Bicrystal Welds', *Metall Trans A*, 1993, **24A**, 1433-1446.

12, S. S. BABU, S. A. DAVID, J.-W. PARK AND J. M. VITEK: 'Joining of Nickel-Base Superalloy Single Crystals', accepted for publication in *Sci Technol Welding Joining*

13. J. D. HUNT: 'Steady State Columnar and Equiaxed Growth of Dendrites and Eutectics', *Mater Sci Eng*, 1984, **65**, 75-83.

14. M. GAÜMANN, C. BEZENÇON, P. CANALIS and W. KURZ: 'Single-Crystal Laser Deposition of Superalloys: Processing-Microstructure Maps', *Acta mater*, 2001, **49**, 1051-1062.

15. J.-W. PARK, S. S. BABU, J. M. VITEK, E.A. KENIK and S. A. DAVID: 'Stray Grain Formation in Single Crystal Ni-Base Superalloy Welds', accepted for publication in *J Appl Phys*

16. T. M. POLLOCK and W. H. MURPHY: 'The Breakdown of Single-Crystal Solidification in High Refractory Nickel-Base Alloys', *Metall Mater Trans A*, 1996, **27A**, 1081-1094.

17. M. GAÜMANN, S. HENRY, F. CLÉTON, J.-D. WAGNIÈRE and W. KURZ: 'Epitaxial Laser Metal Forming: Analysis of Microstructure Formation', *Mater Sci Eng A*, 1999, **A271**, 232-241.